



ELASTIC-PLASTIC CONSTITUTIVE MODEL FOR COHESIONLESS GRANULAR MATERIALS

Dragan Rakić¹, Miroslav Živković¹, Milan Bojović¹

¹ Faculty of Engineering,
University of Kragujevac, Sestre Janjić 6, 34000 Kragujevac
e-mail: drakic@kg.ac.rs

Abstract:

The paper presents development and numerical implementation of elastic-plastic constitutive model for cohesionless granular materials. This constitutive model based on the hyperbolic failure envelope was developed using theory of incremental plasticity. Developed constitutive model contains three material parameters which can be obtained using results of direct shear test or triaxial test of material sample. In stress integration procedure, for system of nonlinear equations solving, governing parameter method was used. Constitutive relations for implicit stress integration are summarized in form of numerical algorithm. Presented algorithm was implemented in the general-purpose finite element program PAK and verified through numerical simulation of the material tests.

Key words: Hyperbolic model, constitutive modelling, granular material, plasticity, PAK

1. Introduction

Numerical analyses of engineering problems are closely related to the choice of appropriate constitutive model used to describe mechanical behavior of analyzed material. Material parameters are determined after adopting the appropriate model. In solving real physical problems, it is convenient to use constitutive models whose parameters are determined using conventional tests of material. It is also necessary for the constitutive model to be sufficiently robust and numerically efficient. In order to satisfy proposed criteria, a constitutive model for cohesionless granular material based on hyperbolic failure surface based on Mohr-Coulomb criteria [1] was developed.

There are numerous suggestions for failure surface description as the function of effective stresses which is divided into parabolic, logarithmic, and hyperbolic shape [2, 3]. However, most of these expressions have disadvantages such as limited stress range, parameter dependence on the stress unit, model parameters without a clear physical meaning, etc. Therefore, the failure surface is important to be defined throughout the range of possible stresses, to be applicable to several types of materials, to have parameters with clear physical meaning, to be consistent with the basic concepts of the accepted theory. On other hand, stress integration is performed for any integration point, so it is essential to have an efficient computational algorithm. Suggested constitutive model is overcoming the problems of the most commonly used constitutive models for cohesionless granular materials.

In the case of implicit stress integration, return mapping algorithm and governing parameter method [4, 5, 6, 7] were used. The methods represent generalization of the radial return method used in general plasticity [8] based on the calculation of the unknown stresses and internal material variables being reduced to the solving one (governing) parameter [9, 10]. Implicit integration method provides that the failure condition is satisfied at the end of each time step. Additionally, the implicit integration methods allow significantly greater time step than explicit integration, leading to faster solution of equation system [11]. Implicit methods are also widespread in solving geotechnical problems [12], as well as in other elastic-plastic and viscoplastic problems [13].

2. Theoretical bases of the model

Constitutive models based on a linear failure envelope are commonly used in numerical simulation of mechanical behavior of granular materials especially for higher stress values. However, linear failure envelope does not describe real mechanical behavior of granular cohesionless material for lower values of normal stress. In order to appropriately describe mechanical behavior for all the possible stress states, Hyperbolic elastic-plastic model was developed. Failure surface of this model resulted from the model with non-linear deformable saw-teeth [14] as presented in Figure 1.

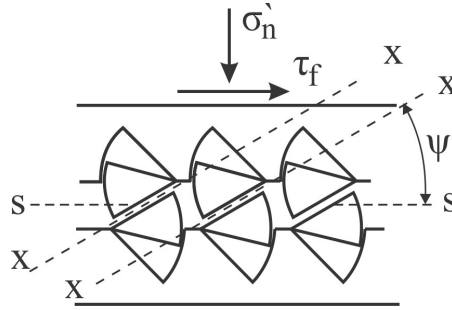


Figure 1 Model with nonlinear deformable saw-teeth

Failure surface of developed model quite realistically describes mechanical behavior of granular materials without cohesion, especially for low stress level. The constitutive model represents the modification of the Mohr-Coulomb model with internal friction angle defined as the function of the stress state. Hyperbolic failure envelope of the model was defined using three material parameters.

Constitutive relations of soil material, as a porous media, describe the laws referring to solid skeleton (effective stress). Effective values of internal variables are usually labelled with the sign prim ($'$), but this sign will be omitted in this paper.

Assuming that there is no cohesion in granular unbounded materials [15, 16], according to [1], shear strength of the material is

$$\tau_f = \sigma_n \tan \phi(\sigma_n) \quad (2.1)$$

Internal friction angle is defined as the function of normal effective stress, so shear strength of the material is

$$\tau_f = \sigma_n \tan \left(\phi_B + \frac{\Delta\phi}{1 + \frac{\sigma_n}{p_N}} \right) \quad (2.2)$$

2.1 Failure surface of the model

Mohr-Coulomb and Hyperbolic model failure surface are the same in case when there is no cohesion. Cohesion in Mohr-Coulomb model is the result of failure envelope linearization and is not the representation of real soil behavior. In case of Hyperbolic elastic-plastic model, internal friction angle is the function of the stress state. Accordingly, failure surface of Hyperbolic elastic-plastic model is defined using Mohr-Coulomb failure surface omitting material cohesion and introducing internal friction angle as the function of the stress state

$$f = \frac{I_1}{3} \sin \phi(\sigma_n) + \sqrt{J_{2D}} \left(\cos \theta - \frac{1}{\sqrt{3}} \sin \theta \sin \phi(\sigma_n) \right) \quad (2.7)$$

Having no hardening feature, failure surface of this constitutive model represents the yield surface at the same time. In the equation (2.7), I_1 represents the first stress invariant, J_{2D} is the second deviatoric stress invariant, θ is Lode's angle, whereas $\phi(\sigma_n)$ represents the internal friction angle defined by the equation (2.5).

3. Implicit stress integration

The equation of failure surface (2.7) represents a composite stress function whose derivative is calculated using the chain rules [18] as

$$\frac{\partial f}{\partial \boldsymbol{\sigma}} = \frac{\partial f}{\partial I_1} \frac{\partial I_1}{\partial \boldsymbol{\sigma}} + \frac{\partial f}{\partial J_{2D}} \frac{\partial J_{2D}}{\partial \boldsymbol{\sigma}} + \frac{\partial f}{\partial \theta} \frac{\partial \theta}{\partial \boldsymbol{\sigma}} + \frac{\partial f}{\partial \phi} \frac{\partial \phi}{\partial \boldsymbol{\sigma}} \quad (2.8)$$

where $\boldsymbol{\sigma}$ represents stress tensor for Cartesian components which in case of isotropic material contain six components.

Individual parts of the equation (2.8) represent derivatives of yield function (2.7) with respect to stress invariants, Lode's angle and internal friction angle as well as individual derivatives are calculated as

$$\frac{\partial f}{\partial I_1} = \frac{\sin \phi}{3} \quad (2.9)$$

$$\frac{\partial f}{\partial J_{2D}} = \frac{1}{2\sqrt{J_{2D}}} \left\{ \cos \theta - \frac{1}{\sqrt{3}} \sin \theta \sin \phi \right\} \quad (2.10)$$

$$\frac{\partial f}{\partial \theta} = -\sqrt{J_{2D}} \left(\sin \theta + \frac{\cos \theta \sin \phi}{\sqrt{3}} \right) \quad (2.11)$$

$$\frac{\partial f}{\partial \phi} = \left(\frac{I_1}{3} - \sqrt{\frac{J_{2D}}{3}} \sin \theta \right) \cos \phi \quad (2.12)$$

Derivatives of the first stress invariant and second deviatoric stress invariant are

$$\frac{\partial I_1}{\partial \boldsymbol{\sigma}} = [1 \ 1 \ 1 \ 0 \ 0 \ 0] \quad (2.13)$$

$$\frac{\partial J_{2D}}{\partial \boldsymbol{\sigma}} = \left[\frac{1}{3}(2\sigma_x - \sigma_y - \sigma_z) \quad \frac{1}{3}(-\sigma_x + 2\sigma_y - \sigma_z) \quad \frac{1}{3}(-\sigma_x - \sigma_y + 2\sigma_z) \quad 2\sigma_{xy} \quad 2\sigma_{yz} \quad 2\sigma_{zx} \right] \quad (2.14)$$

derivative of internal friction angle with respect to stress is

$$\frac{\partial \phi^T}{\partial \boldsymbol{\sigma}} = \begin{bmatrix} -\frac{3\Delta\phi p_{AV}}{(I_1 + 3p_{AV})^2} & -\frac{3\Delta\phi p_{AV}}{(I_1 + 3p_{AV})^2} & -\frac{3\Delta\phi p_{AV}}{(I_1 + 3p_{AV})^2} & 0 & 0 & 0 \end{bmatrix} \quad (2.15)$$

whereas derivative of Lode's angle can be calculated using the chain rule as previously presented.

Algorithm presented in the following section summarizes the steps for stress integration using this model. In order to perform implicit stress integration of Hyperbolic elastic-plastic model, return mapping algorithm was developed [8, 9] and it is presented in Table 1.

<p>Known: ${}^{t+\Delta t} \mathbf{e}$, ${}^t \mathbf{e}$, ${}^t \boldsymbol{\sigma}$, ${}^t \mathbf{e}^p$</p> <p>A. Trial solution: $d\boldsymbol{\sigma} = \mathbf{C}^E d\mathbf{e}^E = \mathbf{C}^E ({}^{t+\Delta t} \mathbf{e} - {}^t \mathbf{e})$, ${}^{t+\Delta t} \boldsymbol{\sigma} = {}^t \boldsymbol{\sigma} + d\boldsymbol{\sigma}$</p> <p>Stress invariants: I_1, J_{2D}, θ</p> <p>Failure and plastic potential function: $f = \frac{I_1}{3} \sin \phi(\sigma) + \sqrt{J_{2D}} \left(\cos \theta - \frac{1}{\sqrt{3}} \sin \theta \sin \phi(\sigma) \right)$</p> <p>B. Yield condition check: IF ($f < 0$) elastic strain (go to E) IF ($f \geq 0$) elastic-plastic strain (CONTINUE)</p> $d\lambda = \frac{\frac{\partial f^T}{\partial \boldsymbol{\sigma}} \mathbf{C}^E d\mathbf{e}}{\frac{\partial f^T}{\partial \boldsymbol{\sigma}} \mathbf{C}^E \frac{\partial f}{\partial \boldsymbol{\sigma}}}$ <p>C. $d\lambda$ correction (local iterations): $d\mathbf{e}^p = d\lambda \frac{\partial f}{\partial \boldsymbol{\sigma}}$, ${}^{t+\Delta t} \boldsymbol{\sigma} = {}^t \boldsymbol{\sigma} + d\boldsymbol{\sigma}$</p> <p>New invariants: I_1, J_{2D}, θ</p> <p>Yield function check: $f = \frac{I_1}{3} \sin \phi(\sigma) + \sqrt{J_{2D}} \left(\cos \theta - \frac{1}{\sqrt{3}} \sin \theta \sin \phi(\sigma) \right)$</p> <p>D. IF ($ABS(f) \geq TOL$) go back to C with new $d\lambda$: ${}^{t+\Delta t} \mathbf{e}^p = {}^t \mathbf{e}^p + d\mathbf{e}^p$</p> <p>E. End: ${}^{t+\Delta t} \boldsymbol{\sigma}$, ${}^{t+\Delta t} \mathbf{e}^p$</p>
--

Table 1 Implicit stress integration algorithm of Hyperbolic elastic-plastic model

In case there are plastic strains in the current time step, yield condition is not fulfilled indicating that total strains are to be corrected by calculating the plastic corrector. Plastic corrector represents the part of plastic strains in total strain. One of the complications in some constitutive model cases can be the complex calculation of yield function and plastic potential derivatives. However, the use of yield function derivatives instead of analytical derivatives overcomes this shortcoming. Presented algorithm is implemented in the program PAK [19] and verified through examples.

4. Verification examples

Two test examples were performed as verification of the developed algorithm for implicit stress integration using Hyperbolic elastic-plastic model. First verification example is numerical simulation of triaxial test with the aim to verify if the developed model accurately describes the

strength of the material sample for given material parameters. Second example represents numerical simulation of direct shear test in order to verify if the developed model accurately describes the mechanical behavior of real samples during shear load. Identification of material parameters was performed using back analysis [20]. Results of numerical simulation were compared with both the analytical and experimental results.

4.1 Triaxial test simulation

Numerical modelling of triaxial test simply verifies whether the developed constitutive model describes the strength of the material in accordance with the theoretical failure criterion for given model parameters. Generally, stress path is classified according to the type and direction of loading. Therefore, the performance of the developed elastic-plastic model for granular material based on hyperbolic failure surface was checked for compression and extension. Four different confining stresses were used. In compression test, the sample was loaded using hydrostatic stress state which was subsequently increased in one direction, whereas it remained constant in the other two directions. In the tension test, to the contrary, the stress was reduced in one direction after set the hydrostatic stress state, while it remained constant in the other two directions.

Used FE model consists of one solid hexagonal finite element with unit dimensions. Figure 3 presents model geometry, boundary conditions and loads. The analyzed model has three planes of symmetry, so accordingly, the appropriate boundary conditions of symmetry were used. Model loads are applied using prescribed pressure in three coordinate directions. The load was increased in multiple steps until inability to achieve convergence of numerical solutions (failure).

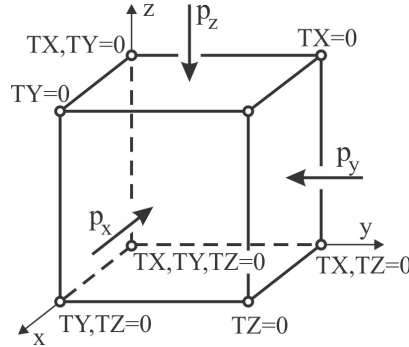


Figure 3. FE model for triaxial test simulation

The procedure was repeated for four levels of confining stress with the aim to confirm that the model provides analytical stress values of the failure for different stress states: $\sigma_m = 0.213$ MPa, 0.421 MPa, 0.839 MPa and 1.665 MPa. In the compression test, the vertical pressure is increased until the failure is reached after reaching the initial stress state. In the extension test, the vertical pressure is reduced until the failure after reaching the initial stress state. Used load functions are presented in Figure 4.

Parameter	Label	Value
Young's modulus	E	20 MPa
Poison's ratio	ν	0.3
Material constant	ϕ_B	17.22°
Material constant	$\Delta\phi$	29.38°
Material constant	p_N	0.62MPa

Table 2. Material parameters used in triaxial test simulation

Report [51] was the source for material parameters used in the numerical simulation of the triaxial test. Used material parameters of the model are presented in Table 2, for the sample RPU-1/98.

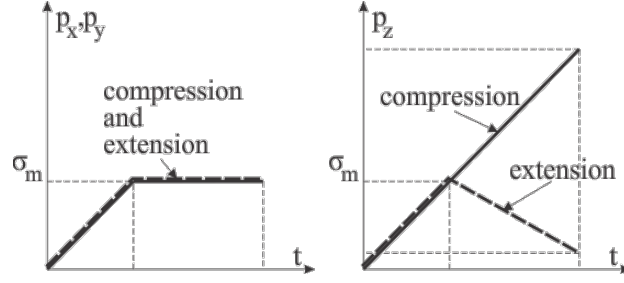


Figure 4. Load functions in triaxial test simulation

Figure 5 presents the simulation results of the triaxial test, for different values of confining pressure in case of compression and extension.

$$q = \sqrt{3J_{2D}} \quad (2.16)$$

The numerical results are presented in the form of stress paths for both analyzed cases and for all confining stresses in the $\sigma_m - q$ stress space, where σ_m represents the mean stress (confining stress) while q represents second invariant of deviatoric stress (2.16).

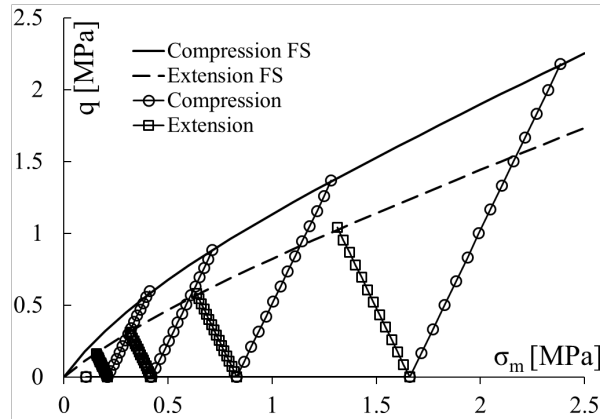


Figure 5. Compression and extension stress path in triaxial test simulation

According to the analysis of the obtained results, the conclusion is that the developed stress at the failure agree with the stress at the failure surface of the Hyperbolic elastic-plastic model. In other words, the developed model describes the strength of the material corresponding to the theoretical values of the failure stress.

4.2 Numerical simulation of direct shear test

This simple numerical simulation is convenient for validation of constitutive model and is used for material parameters identification. Analyzed material represents the rock-fill of the dam's downstream slope, making the application of the Hyperbolic soli model suitable for the numerical simulation. Experimental results of direct shear test of embankment dam supporting body material [21] are presented in Table 3 and used for model parameters identification.

Block No.	σ_n [kPa]	τ [kPa]
1	213	170
2	421	307
3	839	454
4	1665	793

Table 3. Measured values of failure shear stress vs. normal stress

The same normal stress values were used in numerical simulation of direct shear test. Estimated material parameters of Hyperbolic elastic-plastic model are presented in Table 4 and failure surface is shown in Figure 6. Such estimated parameters were used in numerical simulation of shear test.

Used FE model consists of one finite element of unite dimensions with boundary conditions and loads presented in Figure 7. Boundary conditions used in numerical simulation correspond to the boundary conditions of the specimen shear layer.

Parameter	Label	Value
Young's modulus	E	20 MPa
Poison's ratio	ν	0.3
Material constant	ϕ_B	17.22°
Material constant	$\Delta\phi$	29.38°
Material constant	p_N	0.62MPa

Table 4. Estimated material parameters of the hyperbolic model

Model loading was conducted in two phases. The first phase indicates that the vertical pressure is specified on the upper surface of the model (p) up to the values of normal stress used in the material test (Table 3).

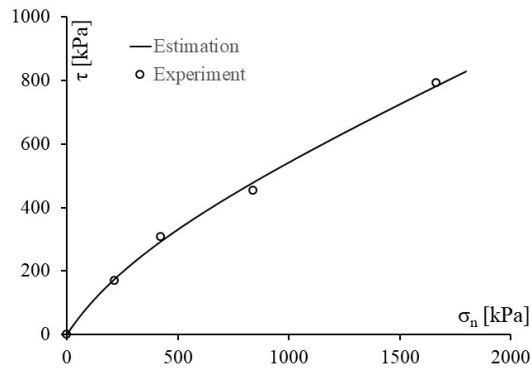


Figure 6. Estimated failure surface

After reaching the specified value of normal stress, horizontal displacement of nodes was applied on the upper model surface (d_x). Load functions used in the test device were the same as the load functions in numerical simulation (Figure 7b).

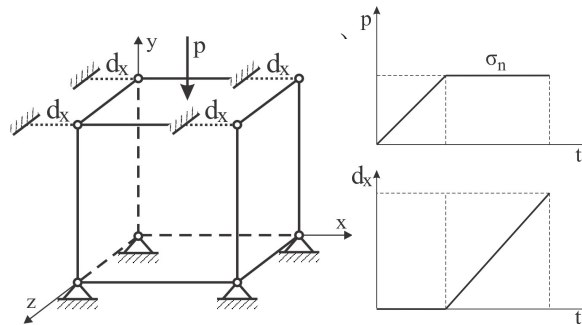


Figure 7. FE model for direct shear test simulation and load functions

Results of numerical simulation and the test results were presented in $\tau_{xy} - e_x$ form (Figure 8). It can be concluded that the developed constitutive model significantly follows the trend of the experimental results through comparing the numerical results obtained using developed algorithm with the experimental results presented in Figure 8. Significant deviations are observed for lower

strain values and are related to the absence of hardening feature in developed model, which could be the subject of further development of the constitutive model.

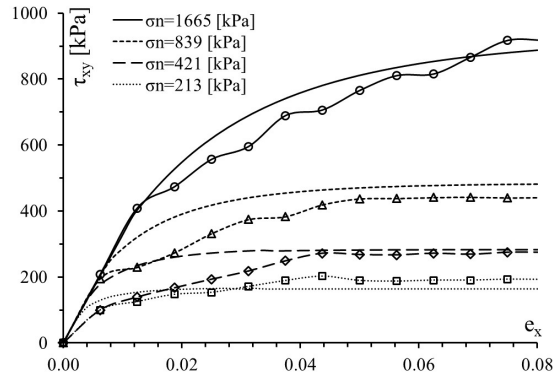


Figure 8. Measured and simulated results of the direct shear test

Parameters of constitutive model can be obtained using direct shear test in large scale. Additionally, developed algorithm for implicit stress integration of Hyperbolic elastic-plastic model obviously well describes mechanical behavior of analyzed material sample in general. Due to the simple reduction of the shear stress envelope, this constitutive model is suitable for the application of shear strength reduction (SSR) method [22] used for factor of safety determination.

5. Conclusions

The paper discusses the development of the constitutive model for cohesionless granular material based on the hyperbolic failure surface using theory of incremental plasticity. Failure surface of the model was defined by modifying Mohr-Coulomb failure surface and introducing internal friction angle as the function of stress state. Model describes more realistic mechanical behavior of cohesionless granular material especially for lower values of confining stress. The model formulation is given and the constitutive relation development for implicit stress integration was presented in details. Failure surface of the model was defined using three material parameters whose meaning was presented in the paper. These material parameters can be obtained using direct shear test or triaxial test. A return mapping algorithm is applied to the model in the general-purpose program PAK. The algorithm was verified through several test examples. Developed model provides good matches of numerical results with analytical results and significantly follows the trend of the experimental results. Some deviations can be observed for lower values of strain as the consequence of the fact that developed model does not have hardening feature which could be the subject of further development of the constitutive model. This confirms applicability of developed model in real geotechnical problem. Suitability for wide applications in engineering problem solving of the Hyperbolic constitutive model based on the nonlinear failure envelope is reflected in the fact that parameters may be obtained directly using standard laboratory tests. Developed model can be improved by introducing a non-associated yield condition. In addition, the model can be modified by introducing a kinematic hardening, so the model can be suitable for dynamic analysis of granular materials. Due to the simplicity of reducing the shear stress envelope, this constitutive model is suitable for the application of shear strength reduction (SSR) method.

Acknowledgements

The part of this research is supported by Ministry of Education and Science, Republic of Serbia, Grant TR32036 and TR37013.

References

- [1] Maksimović, M.: Nonlinear Failure Envelope for Soils, *Journal of Geotechnical Engineering*, 115, 4, pp. 581-586, 1989.
- [2] Barton, N., Kjaernsli, B.: Shear Strength of Rockfill, *Journal of the Geotechnical Engineering Division*, 107: 7, pp. 873-891, 1981.
- [3] Charles, J. A., Watts, K. S.: The influence of confining pressure on the shear strength of compacted rockfill, *Géotechnique*, 30: 4, pp. 353-367, 1980.
- [4] Kojić, M.: The governing parameter method for implicit integration of viscoplastic constitutive relations for isotropic and orthotropic metals, *Computational Mechanics*, 19, pp. 49-57, 1996.
- [5] Simo, J. C., Taylor, R.: Consistent Tangent Operators for Rate-independent Elastoplasticity, *Computer Methods in Applied Mechanics and Engineering*, 48: 1, pp. 101-118, 1985.
- [6] Simo, J. C., Taylor, R.: A return mapping algorithm for plane stress elastoplasticity, *International Journal for Numerical Methods in Engineering*, 22: 3, p. 649-670, 1986.
- [7] Jeremic, B.: *Lecture Notes on Computational Geomechanics*, University of California at Davis, 2010.
- [8] Wilkins, M. L.: *Calculation of elastic-plastic flow*, Livermore, California: University of California, Lawrence Radiation Laboratory, 1963.
- [9] Bathe, K. J., Chaudhary A. B., Dvorkin, E. N., Kojić, M.: On the Solution of Nonlinear Finite Element Equations, *Proceedings of the Int. Conference on Computer-Aided Analysis and Design of Concrete Structures*, Split, Croatia, 1984.
- [10] Kojic, M., Bathe, K. J.: *Inelastic Analysis of Solids and Structures*, 1 edition, Springer, 2004.
- [11] Dunne, F., Petrinic, N.: *Introduction to Computational Plasticity*, Oxford University, 2005.
- [12] Sheng, D., Sloan, S. W., Gens, A., Smith D. W.: Finite element formulation and algorithms for unsaturated soils. Part I: Theory, *International Journal for Numerical and Analytical Methods in Geomechanics*, 27: 9, p. 745-765, 2003.
- [13] Zhang, C., Ji, J., Yang, S.Q., Kodikara J.: Implicit integration of simple breakage constitutive model for crushable granular materials: A numerical test, *Computers and Geotechnics*, 82, pp. 43-53, 2017.
- [14] Patton, F. D.: Multiple Modes of Shear Failure In Rock, 1st ISRM Congress-International Society for Rock Mechanics, Lisbon, Portugal, 1966.
- [15] Duriez, J., Vincens, É.: Constitutive modelling of cohesionless soils and interfaces with various internal states: An elasto-plastic approach, *Computers and Geotechnics*, 63: 33-45, 2015.
- [16] Bolton, M. D.: The Strength and Dilatancy of Sands, *Geotechnique*, 1: 36, pp. 65-78, 1986.
- [17] Maksimović, M.: *Soil mechanics*, fourth edition, AMG book, Belgrade, 2008.
- [18] Bronshtein, I., Semendyayev, K., Musiol, G.i Muehlig, H.: *Handbook of Mathematics*, Frankfurt am Main, Wissenschaftlicher Verlag Harrz Deutch GmbH, 2005.
- [19] Kojić, M., Slavković, R., Živković, M., Grujović, N.: PAK-finite element program for linear and nonlinear structural analysis and heat transfer, University of Kragujevac, Faculty of Engineering, Kragujevac.
- [20] Vahdati, P.: Identification of soil parameters in an embankment dam by mathematical optimization, Luleå University of Technology, Luleå, Sweden, 2014.
- [21] Jaroslav Cerni Institute for the Development of Water Resources: Elaborate on geological research results – Preliminary project, Belgrade, Serbia, 2011.
- [22] Berisavljević, Z., Berisavljević, D., Čebašek, V., Rakić, D.: Slope stability analyses using limit equilibrium and soil strength reduction methods, *Građevinar*, 67: 10, pp. 975-983, 2015.